ACS Catalysis

pubs.acs.org/acscatalysis Research Article

Pincer−Ruthenium-Catalyzed Reforming of Methanol—Selective High-Yield Production of Formic Acid and Hydrogen

Vinay Arora, Eileen Yasmin, Niharika Tanwar, Venkatesha R. Hathwar, Tushar Wagh, Sunil Dhole, and Akshai Kumar*

Cite This: *ACS Catal.* 2023, 13, 3605−3617 Read Online

ACCESS | Metrics & More | Article Recommendations | Supporting Information

ABSTRACT: A series of NNN pincer−ruthenium complexes of the type (^{R2}NNN)RuCl$_2$(CH$_3$CN) based on *bis*(imino)pyridine ligands were synthesized and characterized. These pincer ruthenium acetonitrile complexes, along with their phosphine and carbonyl counterparts, were tested for the reforming of methanol in water in the presence of a base. The catalyst (^{Cy2}NNN)-RuCl$_2$(PPh$_3$) was found to be the most efficient in comparison to other considered catalysts. Among the bases screened, KO^{t}Bu (1.5 equiv with respect to water) was found to give the best results at temperatures as low as 100 °C. Under these conditions, while (^{Cy2}NNN)RuCl$_2$(PPh$_3$) (0.2 mol %) in a mixture of methanol and water in a 2:1 ratio gave a yield of up to 81% each of hydrogen and formic acid (FA) at 100% selectivity, the corresponding reaction with 2 mol % (^{Cy2}NNN)RuCl$_2$(PPh$_3$) gave up to 90% of hydrogen and 73% of FA at 80% selectivity. On the other hand, the (^{Cy2}NNN)RuCl$_2$(PPh$_3$) (0.8 mol %) catalyzed reforming of a 3:1 methanol/water mixture gave good yields (84%) of hydrogen with 81% FA at 95% selectivity. The yield of hydrogen was cross-verified by using it to reduce unsaturated compounds and determining the corresponding yield of the reduced product, which was found to be consistent. Isotope-labeling studies suggest the involvement of C−H activation as a part of the catalytic cycle and not as a part of the rate-determining step (RDS) with an average secondary KIE of 1.96. The reaction was observed to have a first-order dependence of rate on the concentration of both (^{Cy2}NNN)RuCl$_2$(PPh$_3$) and methanol. DFT studies are in agreement with this, and the σ-bond metathesis leading to the elimination of the first molecule of hydrogen is computed to be the RDS either for the cycle leading to FA and 2 moles of hydrogen or for the cycle that results in carbon dioxide and 3 moles of hydrogen. The Ru−H species (^{Cy2}NNN)RuCl(H) plays a decisive role in the unprecedented selectivity toward FA. In its choice to undergo a σ-bond metathesis either with the O−H of methanol (that completes the FA cycle) or with the O−H of FA that leads to carbon dioxide, it chooses the former as it is kinetically more favored by 4.58 kcal/mol. The current catalytic system comprising of NNN pincer-ruthenium phosphines based on *bis*(imino)pyridine ligands that gives high yields of H$_2$ and FA at unprecedented selectivity at low operating temperature offers immense promise in the transformation of methanol to clean-burning hydrogen and high-value FA.

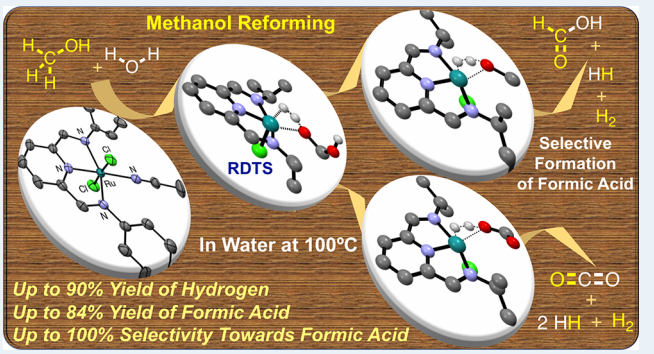

KEYWORDS: *pincer−ruthenium complexes, dehydrogenation, hydrogen, formic acid, methanol and DFT studies*

INTRODUCTION

Due to the ever-increasing global energy demand and the rapid rate at which fossil fuel reserves are being depleted, there is a great need for the emergence of alternative and clean sources of energy which are sustainable and also would lessen the burden of global pollution.[1] Alternative energy sources explored till date, like solar, wind, tidal, nuclear, and geothermal, suffer from several limitations.[2] Thus, a realistic alternative would be utilizing a combination of renewable energy sources and fossil fuels, leading to an uninterrupted production and storage of energy.[3a−c] Several reports have emerged over the last few years on the production of H$_2$ as a clean-burning sustainable energy source with high energy content (120 MJ/kg).[3d−g] Globally, the current emphasis is on sustainable hydrogen production from biomass[3h,i] or via thermochemical, photocatalytic, or electrolytic splitting of water[3h−j] using electricity from wind,[3k,l] solar,[3k,l] and geothermal energy.[3h,i,m−o] The significant advancement in green hydrogen production is, to a large extent, overshadowed by the limitations associated with its storage and transportation, which include but are not limited to low volumetric energy

Received: November 14, 2022
Revised: February 15, 2023
Published: February 27, 2023

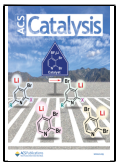

https://doi.org/10.1021/acscatal.2c05587
ACS Catal. 2023, 13, 3605−3617

density, safe handling, and the need for expensive cryogenic and high-pressure compression cylinders.[3p−s] Alternative hydrogen adsorption-based technologies suffer from drastic conditions, low hydrogen storage capacities, low energy efficiency, and high cost.[3t,u] An emerging area of hydrogen carrier systems is its storage in the chemical bonds of tiny organic molecules.[3b,v,w] This is typically accomplished by catalytic dehydrogenation of light organic hydrogen carriers.[3b,v,w] Among the various catalysts that are at one's disposal, homogeneous catalysts, especially those based on pincers (chelating ligands that bind the metal through three adjacent donor sites in a meridional geometry) have been efficient in catalyzing reactions involving the release of hydrogen, such as the aqueous reforming of methanol (Scheme 1).[3]

Scheme 1. Schematic Representation of Methanol Reforming

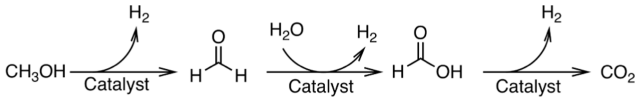

Methanol has up to 12.6% H_2 content and hence has been used as an efficient hydrogen storage medium as it is capable of meeting the ultimate Department of Energy targets (5.5 wt %) for H_2 storage on-board vehicles.[3d] Rightly, its reforming has been reported by a number of groups employing homogeneous complexes, resulting in hydrogen production in high yields and TON. A major report that emerged in 2013 independently by the groups of Beller[4] and Grutzmacher[5] describes the use of Ru complexes for the catalytic conversion of the MeOH/H_2O mixture to H_2 and CO_2 (or CO_3^{2-}).

Beller[4] demonstrated that, in the presence of the Ru−MACHO pincer complex (**B**) and base, methanol is dehydrogenated to formaldehyde, which, in presence of water, is further dehydrogenated to formic acid (FA) and finally to carbon dioxide. Three equivalents of H_2 are evolved in the process, at an ambient temperature of 65−90 °C, to give a total a TON of 353409 at a TOF of 4700 TO/h.[4] In the same year, an anionic Ru complex (**C**) was reported by Grutzmacher for methanol reforming, yielding a lower TOF (54 TO/h) than the former but at a higher methanol conversion (ca. 84% yield of H_2).[5] This reaction proceeded without the additional use of base, and the H_2/CO_2 gas mixture evolved was able to power an H_2/O_2 fuel cell. Later, they proceeded to elucidate the mechanistic details of the reaction involving the complex [Ru(trop2dad)], trop2dad = 1,4-*bis*(5H-dibenzo[*a*,*d*]cyclohepten-5-yl)-1,4-diazabuta-1,3-diene) by density functional theory (DFT)-based molecular dynamics and solvent effects.[6] Meijer and co-workers also focused their study on the solvent effects of this reaction, concluding that the involvement of polar protic solvents largely influences the energetics of the reaction due to hydrogen bonding with the solvent molecules.[7] Other significant Ru-based catalysts for this reaction include those by Beller [Ru-MACHO (**B**) and pincer ruthenium bisphosphine dihydride complex (**D**) that give 2064 TON and 2392 TON, respectively][8] and Milstein's PNN pincer−ruthenium complex (**F**) that results in up to 29,000 TON.[9]

In 2021, Singh and co-workers demonstrated the methanol reforming at low temperatures (90−130 °C) employing in situ generated Ru nanoparticles from the ruthenium precursor **E** .[10] Acridine-based pincer−ruthenium complex (**G**) has recently been reported by Milstein for the base-free aqueous methanol reforming process, and a very high reactivity was observed with the addition of catalytic amount of hexanethiol.[11] They obtained very high TONs of H_2 (up to 130,000) after weeks of heating. DFT and experimental studies pointed toward the involvement of the ruthenium−thiolate complex (**G**) as the catalytically active species responsible for the outer-sphere dehydrogenation of methanol and methanediol. Recently, Qin, Chung, Zheng, and co-workers applied the third generation Grubbs catalysts (**H**) for the hydrogen production and achieved 158 TO/h and 11424 TON after 72 h.[12] Notably, under homogeneous conditions, while methanol reforming is dominated by catalysts based on Ru, there are a few reports with catalysts based on Rh,[13,14] Ir,[15−17] Fe,[18,19] and Mn,[20] most of which, barring catalyst **I** (Figure 1), are selective toward carbon dioxide production.

In the context of the role of pincer−metal complexes in catalytic reforming of methanol, it is noteworthy that majority of the reports involve moderately good π-accepting phosphine flanking groups in combination with a central N that is either a σ-donating amine or a pyridyl N.[3a] As the modification of pincer donor atoms have a profound impact on the catalytic activity, it would be interesting to probe the change in reactivity when the π-accepting phosphine flanking groups are replaced by σ-donor groups (say weaker σ-donor imines to begin with), while keeping the central pyridyl N intact. The resulting *bis*(imino)pyridine based NNN pincers would be innocent that offer a distinctly different metal-centered reactivity in stark contrast to the corresponding phosphine-based ligands which are typically noninnocent and operate via metal−ligand cooperation.[3a]

The NNN pincer ligands employed in the current report are innocent, and the reactivity is expected to be metal-centered. Our group has previously reported a series of NNN pincer−ruthenium complexes (**1a−f** and **2a−f**, Figure 2) based on *bis*(imino)pyridine and 2,6-*bis*(benzimidazole-2-yl) pyridine ligands for catalytic reactions like *N*-alkylation,[21] glycerol transformation to lactic acid,[22] β-alkylation,[23] and Guerbet reactions[23] that involve dehydrogenation as a key step in the presence of varying amounts of base. Considering the fact that methanol reforming by homogeneous catalysts[4−20] also involves its dehydrogenation in the presence of typical bases as promoters, these NNN pincer−ruthenium complexes (**1a−f** and **2a−f**, Figure 2) are likely to be potential catalyst candidates for this valuable transformation. In addition, a series of new pincer−ruthenium complexes (**3a−c**, Figure 2) were synthesized and employed for catalytic methanol reforming. In stark contrast to the other catalysts reported for methanol reforming (**A−O**, Figure 1) that are mostly selective toward carbon dioxide (barring **E** and **I**), the considered catalysts [(^{Cy2}NNN)$RuCl_2PPh_3$ (**2b**) in particular, Figures 1 and 2] resulted in the selective production of FA along with the concomitant evolution of hydrogen in unprecedented yields. Considering the precious nature of FA[3x−z] and the hazardous nature of greenhouse carbon dioxide, the current report offers immense potential for the value addition of methanol reforming via selective production of FA along with the generation of clean-burning hydrogen.

RESULTS AND DISCUSSION

Synthesis and Characterization of Pincer−Ruthenium Acetonitrile Complexes Based on *bis*(Imino)pyridine

https://doi.org/10.1021/acscatal.2c05587
ACS Catal. 2023, 13, 3605−3617

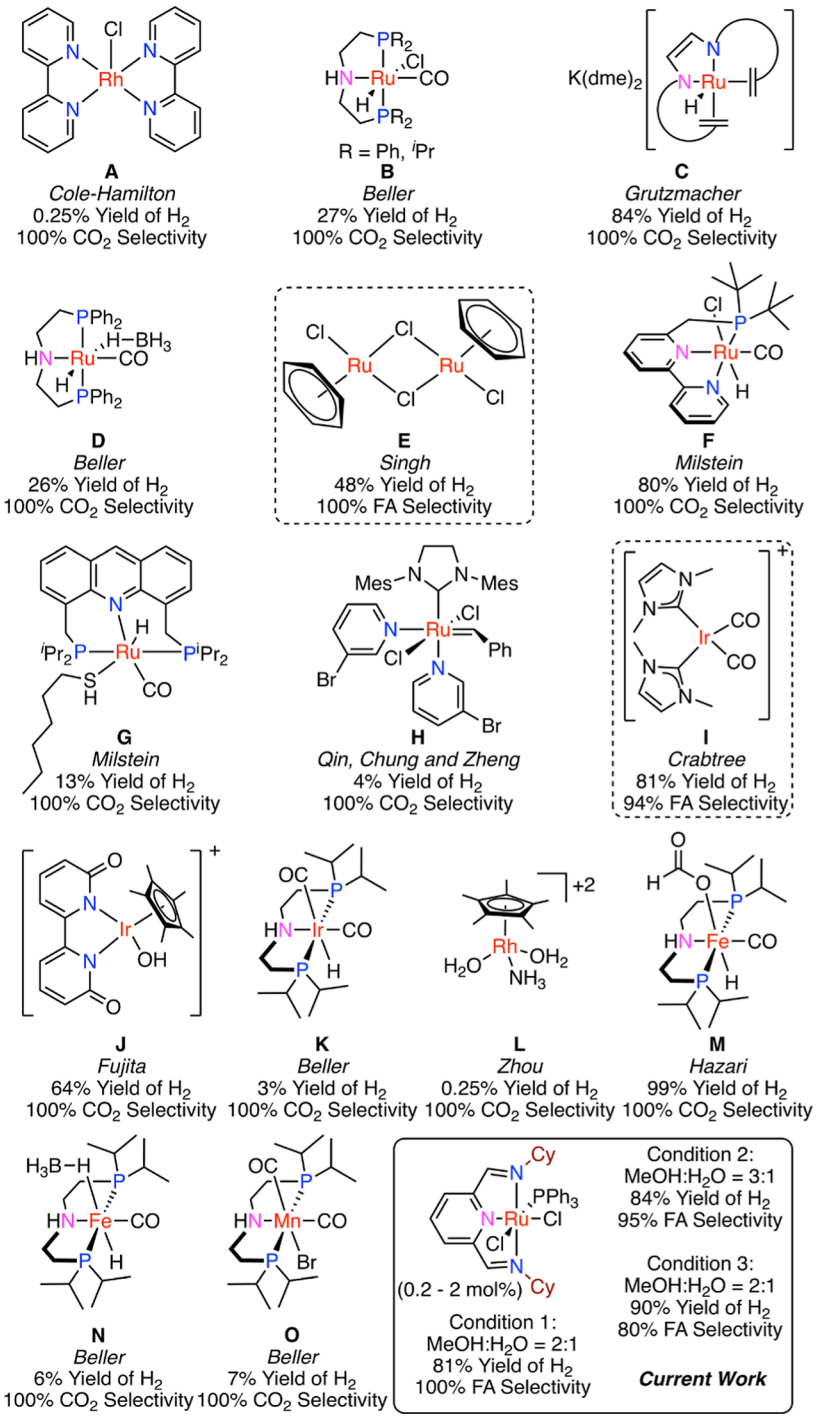

Figure 1. Homogeneous catalysts reported for the methanol reforming reaction.

Ligands. The NNN pincer−Ru acetonitrile complexes (**3a**−**c**) were synthesized in good yields by the treatment of the corresponding ligands[21−24] with $[Ru(p\text{-cymene})Cl_2]_2$ in acetonitrile under reflux conditions overnight, followed by washing with diethyl ether (Scheme 2). The complexes **3a**−**c** were fully characterized by high-resolution mass spectrometry (HRMS) and infrared (IR), ^1H, and ^{13}C nuclear magnetic resonance (NMR) studies.

Good-quality single crystals were obtained by slow diffusion of 1 mL pentane into a 1 mL dichloromethane solution of 10 mg of the pincer−ruthenium complex **3c**. We were also successful in obtaining well-defined single crystals of **2f**, which was elusive in our previous attempts mainly due to its poor solubility. The structures of both **3c** and **2f** were unambiguously determined by single-crystal X-ray diffraction studies. The structure with ORTEP drawn at 50% probability is provided in Figure 3. The phenyl groups on all phosphorus, all the hydrogen atoms, and the solvent molecules are omitted for the sake of clarity.

Catalytic Activity of Pincer−Ruthenium Complexes (1, 2, and 3) toward a Aqueous-Phase Methanol Reforming Reaction. The initial optimization of pincer−ruthenium (**1**, **2**, and **3**) catalyzed aqueous-phase methanol reforming was commenced by heating a mixture of MeOH and

https://doi.org/10.1021/acscatal.2c05587
ACS Catal. 2023, 13, 3605−3617

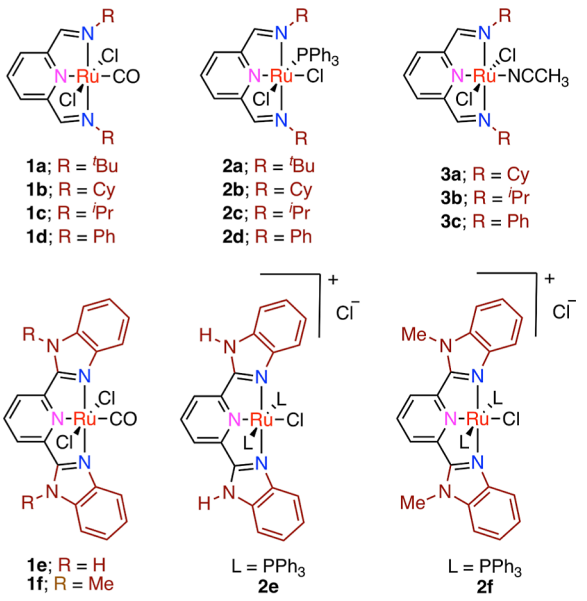

Figure 2. NNN pincer−ruthenium catalysts investigated in the current study for the methanol reforming reactions.

Scheme 2. General Synthetic Route to NNN Pincer−Ruthenium Acetonitrile Complexes

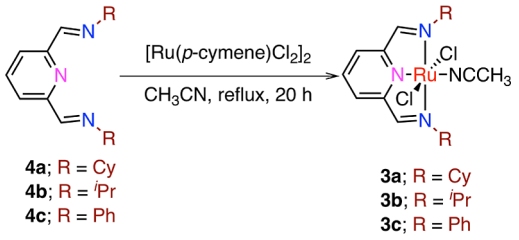

H_2O (in a 2:1 ratio) containing an equivalent of base (with respect to water) in the presence of 0.04 mol % of

Table 1. 1b Catalyzed Aqueous-Phase Methanol Reforming in the Presence of Various Bases[a]

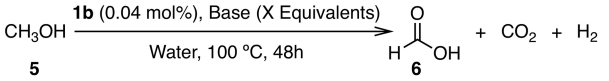

			% yield of products		
entry	base (*X* equiv)	mmol of gas	H_2[b]	HCOOH[c]	CO_2[d]
1	NaOH (1)	0.17	1.89	1.89	0
2	NaO^{t}Bu (1)	0.14	1.48	1.48	0
3	KO^{t}Bu (1)	0.37	3.4[e]	2.2	1.2
4	NaOEt (1)	0.23	2.5	2.5	0
5	Na_2CO_3 (1)	0.04	0.42	0.42	0
6	K_2CO_3 (1)	0.05	0.6	0.6	0
7	KOH (1)	0.03	0.3	0.3	0
8	NaO^{t}Bu (0.2)	0.15	1.63	1.63	0
9	KO^{t}Bu (0.5)	0.31	3.29	3.29	0
10	KO^{t}Bu (0.2)	0.12	1.28	1.28	0
11	KO^{t}Bu (0.1)	0.01	0.1	0.1	0

[a]Reaction conditions: methanol (0.375 mL, 9.27 mmol), H_2O (0.083 mL, 4.635 mmol), base (*X* equiv), and **1b** (0.04 mol %) at 100 °C. Gas evolution was determined by burette measurements. [b]Yield was calculated as moles of H_2 (as determined from GC and the amount of gas evolved, see page S2)/moles of H_2O. [c]The yield of FA is calculated by ^{1}H NMR spectroscopy using sodium acetate as an internal standard. [d]The amount of carbon dioxide formed in the reaction was calculated from SE1 and determined from GC (see page S2). [e]Calculated as weighted average of % hydrogen generated from FA and % hydrogen generated from carbon dioxide, as shown in SE2 (see page S2).

^{Cy2}NNNRuCl$_2$(CO) (**1b**) as the catalyst (Table 1) at 100 °C. Among the various bases screened, KO^{t}Bu showed better reactivity (entry 3 vs entries 1−7, Table 1). When the reaction was further optimized at various loadings of KO^{t}Bu, the best

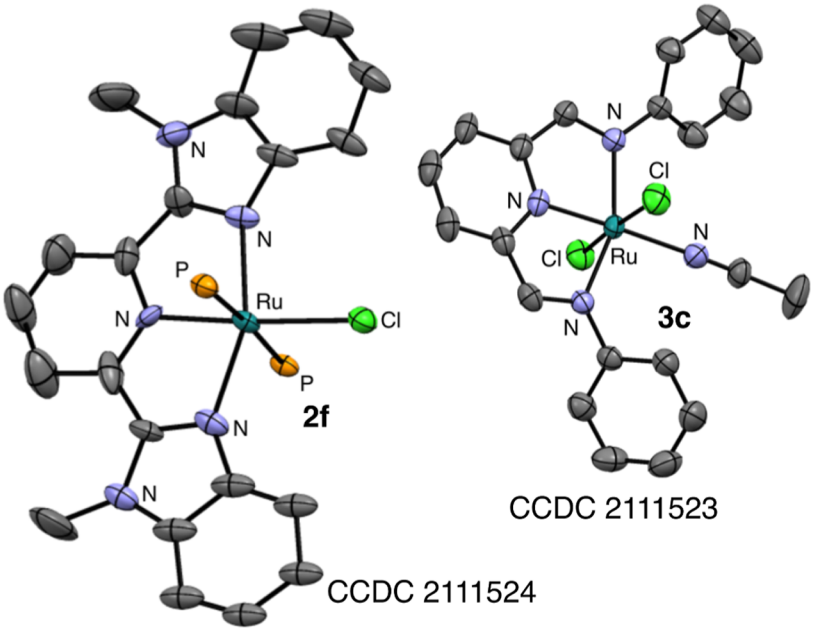

Figure 3. Crystal structures of **2f** and **3c** with ORTEP drawn at 50% probability. The phenyl groups on all phosphorus, all the hydrogen atoms, and the solvent molecules are omitted for the sake of clarity.

https://doi.org/10.1021/acscatal.2c05587
ACS Catal. 2023, 13, 3605−3617

result was obtained while using 0.5 equiv of KO^{t}Bu (entry 9 vs entries 3, 10, and 11, Table 1).

Further optimization of various pincer−ruthenium catalysts was carried out with MeOH and H_2O in a 2:1 ratio using 0.5 equiv of KO^{t}Bu (Table 2). The best catalytic activity among

Table 2. Aqueous-Phase Methanol Reforming Catalyzed by Various Ruthenium Complexes in the Presence of KO^{t}Bu[a]

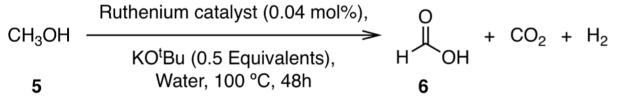

entry	catalyst (0.04 mol %)	mmol of gas	% yield of products H_2[b]	HCOOH[c]	CO_2[d]
1	**1a**	0.1	1	1	0
2	**1b**	0.31	3	3	0
3	**1c**	0.1	1	1	0
4	**1d**	1.3	14	14	0
5	**1e**	0.1	1	1	0
6	**1f**	0.8	9	9	0
7	**2a**	0.2	3	3	0
8	**2b**	2.2	24	24	0
9	**2c**	0.7	8	8	0
10	**2d**	1.9	21	21	0
11	**2e**	0.7	8	8	0
12	**2f**	1.2	13	13	0
13	**3a**	0.6	7	7	0
14	**3b**	0.5	6	6	0
15	**3c**	0.2	2	2	0
16	$RuCl_2(PPh_3)_3$	0.2	3	3	0
17	$RuCl_3{\cdot}3H_2O$	0.4	2.5[e]	1	1.5
18	$[Ru(p\text{-cymene})Cl_2]_2$	1.09	12	12	0

[a]Reaction conditions: methanol (0.375 mL, 9.27 mmol), H_2O (0.083 mL, 4.635 mmol), base (0.5 equiv), and Ru catalyst (0.04 mol %) at 100 °C. Gas evolution was determined by burette measurements. [b]Yield was calculated as moles of H_2 (as determined from GC and the amount of gas evolved, see page S2)/moles of H_2O. [c]The yield of FA is calculated by ^{1}H NMR spectroscopy using sodium acetate as an internal standard. [d]The amount of carbon dioxide formed in the reaction was calculated from SE1 and determined from GC (see page S2). [e]Calculated as weighted average of % hydrogen generated from FA and % hydrogen generated from carbon dioxide, as shown in SE2 (see page S2).

the carbonyl complexes (**1a−f**) was exhibited by ^{Ph2}NNNRuCl$_2$(CO) (**1d**) which gave yields of hydrogen and FA that were about 4.7 folds (entry 4 vs entry 2, Table 2) higher in comparison to that obtained with **1b**. On the other hand, the corresponding yields obtained with **1a**, **1c,** and **1e** were about three-folds (entries 1, 3, and 5 vs entry 2, Table 2) lower. Further, upon employing the analogous PPh_3 complexes **2a−f** (Table 2, entries 7−12), better yields (ca. 23.7% each, 7.9 folds higher in comparison with **1b**) of hydrogen and FA were obtained with complex **2b** (entry 8 vs entry 2, Table 2). The corresponding yields obtained in the reaction catalyzed by **2d** were comparable (ca. 21%, entry 10 vs entry 8, Table 2). The reactivity of **2f** was comparable to **1d** (entry 12 vs entry 4, Table 2) The corresponding acetonitrile analogues (**3a−c**) gave lower yields (entries 13−15, Table 2) in comparison to **2a−d**. The commercially available ruthenium precursors $RuCl_3{\cdot}3H_2O$, $RuCl_2(PPh_3)_3$ and $[Ru(p\text{-cymene})Cl_2]_2$ demonstrated lower reactivity in comparison to the corresponding pincer−ruthenium complexes (entries 16−18, Table 2).

Among all the complexes screened, ^{Cy2}NNNRuCl$_2$(PPh$_3$) (**2b**) turned out to be the most active catalyst (23.7% yield of H_2 and HCO_2H, entry 8, Table 2).

Further variations in reaction conditions (Table 3) were performed with 0.04 mol % loading of **2b** and 0.5 equiv KO^{t}Bu

Table 3. Aqueous-Phase Methanol Reforming Catalyzed by 2b under Various Conditions

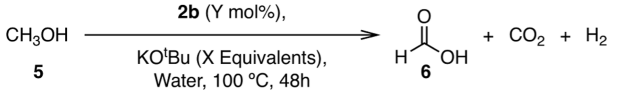

entry	**2b** (Y mol %)	KO^{t}Bu (X equiv)	mmol of gas	% yield of products H_2[b]	HCOOH[c]	CO_2[d]
1[a]	0.04	0.5	2.2	24	24	0
2[a,e]	0.04	0.5	2.14	23	23	0
3[a,f]	0.04	0.5	1.91	21	21	0
4[a]	0.04	1.0	3.98	43	43	0
5[g]	0.04	1.5	3.04	66	66	0
6[g]	0.1	1.5	3.2	69	69	0
7[g]	0.2	1.5	3.8	81[i]	81	0
8[g]	0.4	1.5	4.98	82[h]	56	24
9[g]	0.8	1.5	5.3	89[h]	64	25
10[g]	2.0	1.5	5.0	90[h]	73	18
11[j]	0.8	1.5	4.05	84[h]	81 ± 2[n]	4
12[k]	0.8	1.5	3.4	51	1	50
13[l]	0.8	0.75	3.4	29	21	8
14[m]	0.8	0.75	0	0	0	0

[a]Reaction conditions: methanol (0.375 mL, 9.27 mmol), H_2O (0.083 mL, 4.64 mmol), base (*X* equiv), and **2b** (*Y* mol %) at 100 °C. Gas evolution was determined by burette measurements. [b]Yield was calculated as moles of H_2 (as determined from GC and the amount of gas evolved, see page S2)/moles of H_2O. [c]The yield of FA is calculated by ^{1}H NMR spectroscopy using sodium acetate as an internal standard. [d]The amount of carbon dioxide formed in the reaction was calculated from SE1 and determined from GC (see page S2). [e]Reaction was performed at 120 °C. [f]Reaction was performed at 140 °C. [g]Reaction conditions: methanol (0.188 mL, 4.64 mmol), H_2O (0.042 mL, 2.32 mmol), base (*X* equiv), and **2b** (*Y* mol %) at 100 °C. Gas evolution was determined by burette measurements. [h]Calculated as weighted average of % hydrogen generated from FA and % hydrogen generated from carbon dioxide, as shown in SE2 (see page S2). [i]This corresponds to 3.8 mmol of hydrogen, which was further confirmed by obtaining 3.8 mmol of ethyl benzene starting from 4 mmol of styrene in the presence of Pd/C at 120 °C. [j]6.95 mmol of MeOH, 2.32 mmol of water, 3.48 mmol of KO^{t}Bu, and 0.018 mmol of **2b** were used. [k]9.268 mmol of MeOH, 2.32 mmol of water, 3.48 mmol of KO^{t}Bu, and 0.018 mmol of **2b** were used. [l]Only MeOH (4.64 mmol) and 0.037 mmol of **2b** were used. [m]Only water (4.64 mmol) and 0.037 mmol of **2b** were used. [n]Average of three runs.

and MeOH/H_2O (2:1). To begin with, the influence of the temperature on the catalytic performance was studied. Notably, the yields of hydrogen and FA at 120 °C and at 140 °C were comparable to those observed at 100 °C in the **2b**-catalyzed aqueous-phase methanol reforming reaction (entries 2 and 3 vs entry 1, Table 3). Hence, further optimizations were performed at 100 °C for the **2b**-catalyzed aqueous-phase methanol reforming reaction. Notably, systematic improvements in yields were observed when the base loading was increased to 1 equiv and further to 1.5 equiv of KO^{t}Bu leading to 43 and 66%, respectively, of hydrogen and FA each (entries 4−5, Table 3). It is noteworthy that, in these

https://doi.org/10.1021/acscatal.2c05587
ACS Catal. 2023, 13, 3605−3617

Scheme 3. Plausible Mechanism Involved in the 2 Catalyzed Reforming of Methanol

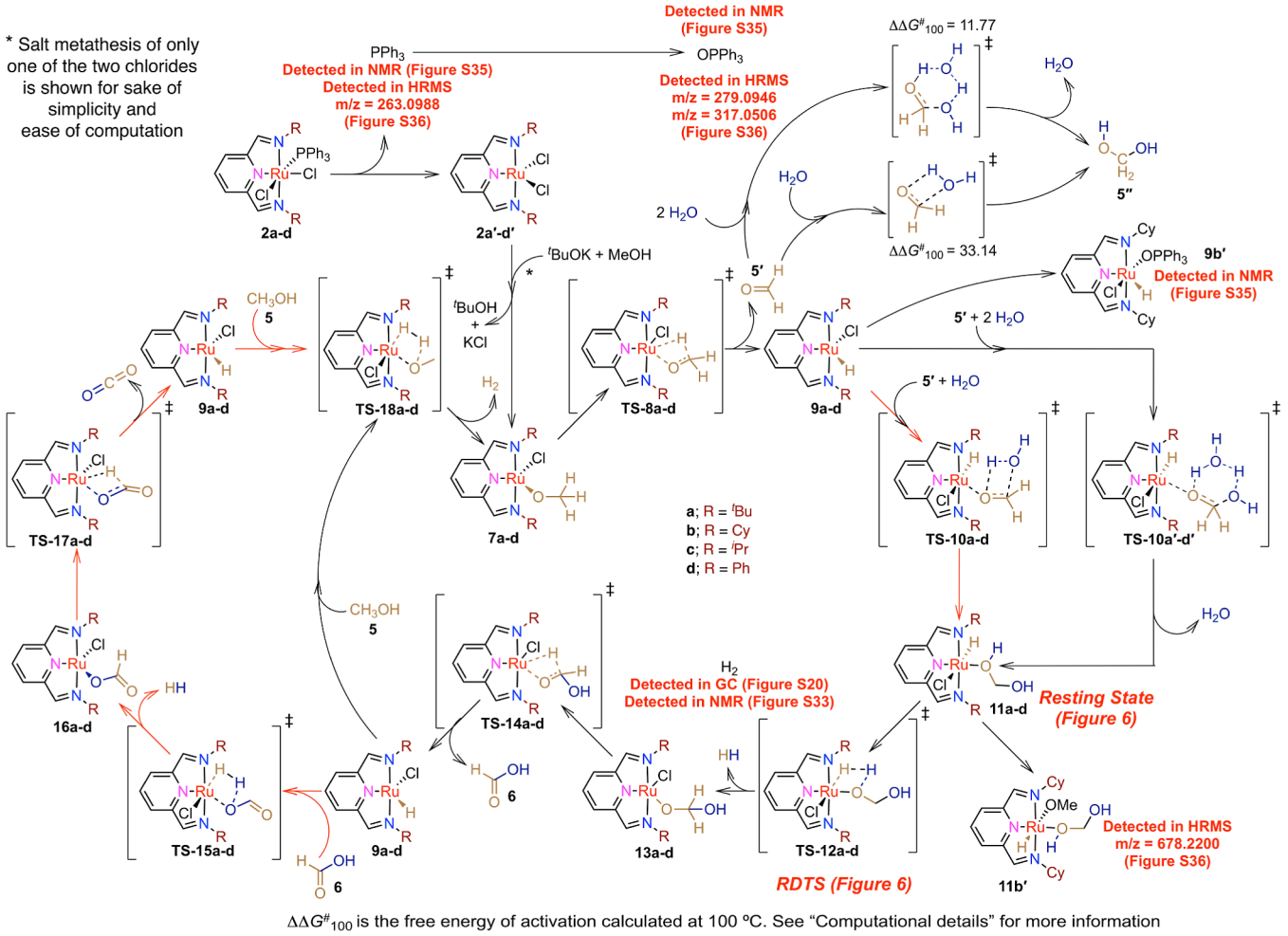

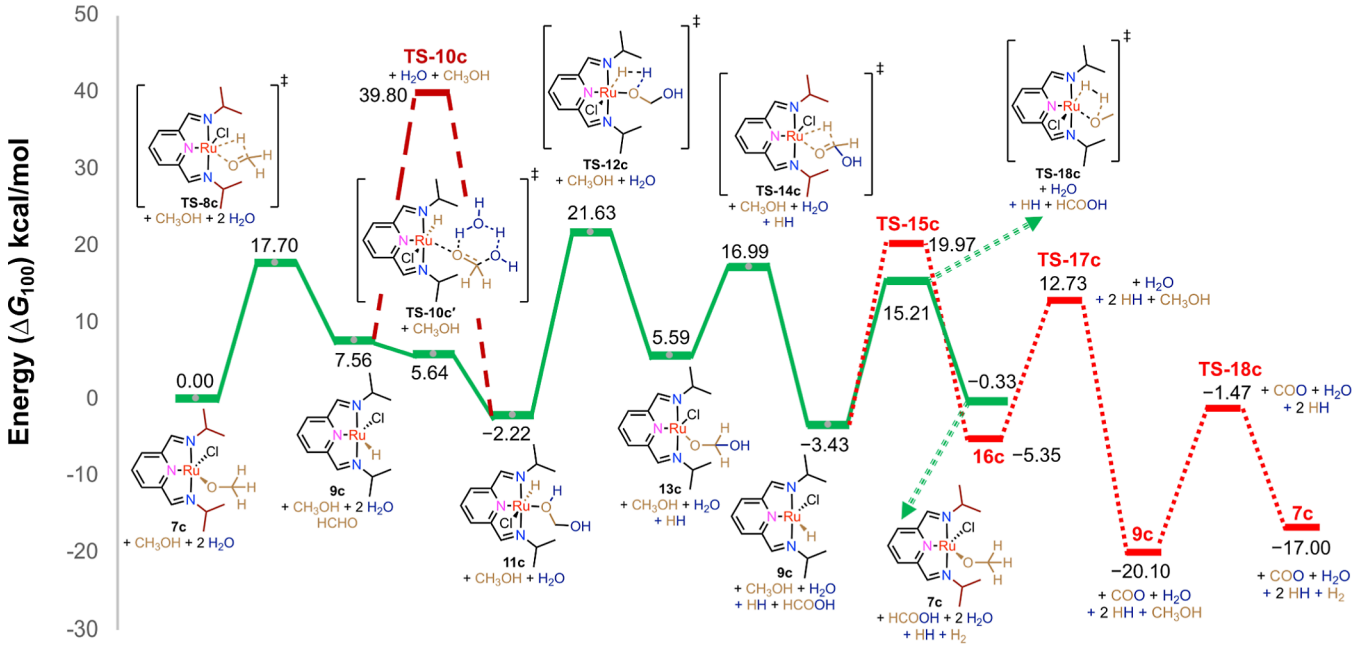

Figure 4. Free energy (ΔG_{100}) profile of the **2c** catalyzed reforming of methanol at 100 °C. Structures of intermediates and transition states of only the favorable path (green solid lines) leading to FA are provided. While the unfavorable path of the methanol to FA transformation is depicted as dark red dashed lines, the path involving the methanol to carbon dioxide conversion is shown as red dotted lines.

https://doi.org/10.1021/acscatal.2c05587
ACS Catal. 2023, 13, 3605−3617

reactions, the selectivity toward FA is almost quantitative. A further increase in base loading was not investigated owing to the poor solubility of KO^{t}Bu at higher concentrations.

There was a gradual increase in yield of hydrogen when the catalyst loading was increased (entries 5−10, Table 3) albeit with a compromise in FA selectivity. The best yield of hydrogen and FA at 100% selectivity toward the latter was about 81% each and was obtained for the reforming of a 2:1 methanol/water mixture containing 1.5 equiv of KO^{t}Bu catalyzed by 0.2 mol % of **2b**. At 0.8 mol % of **2b**, though hydrogen was obtained in a yield of 89%, the yield of FA was however low (64 at 72% selectivity) owing to subsequent dehydrogenation to carbon dioxide (ca. 25%, entry 9, Table 3). There was hardly any increment in yield when the reaction was repeated with 2 mol % of **2b**, ultimately leading to 90% hydrogen and 73% FA at 80% selectivity (entry 10, Table 3).

The generation of hydrogen from aqueous methanol was studied at higher concentrations of methanol (ca. 3:1 with respect to water), and good yields (84%) of hydrogen along with 82% of FA at 95% selectivity was achieved (entry 11, Table 3). Further increase in methanol/H_2O to 4:1 lead to lower yields of hydrogen with no selectivity toward FA (entry 12, Table 3). Lower yields of hydrogen were observed in case of neat methanol highlighting the importance of water in the reaction (entry 13, Table 3). On the other hand, no reaction was observed when only water was used as the reactant (entry 14, Table 3).

Control Experiments and Mechanistic Studies on the Pincer−Ruthenium Catalyzed Aqueous-Phase Methanol Reforming Reaction. Scheme 3 depicts the proposed mechanism catalyzed by **2a−d**, which demonstrates fairly good activity among all the considered catalysts. In an influential pioneering computational study, Lei very nicely elucidates the nature of the pincer−ruthenium catalyzed aqueous-phase methanol dehydrogenation to carbon dioxide and dihydrogen.[4b] We set up on to computationally probe the factors that influence the selective formation of FA that is observed in the current study on pincer−ruthenium catalyzed aqueous-phase methanol dehydrogenation. For this purpose, DFT calculations were performed employing the PBEPBE method using the Def2SVP basis set with a polarization function (Figure 4).

The first step involves the loss of PPh_3 from **2c** to afford a 16-electron pentacoordinate species consisting of two chloride ligands (**2c′**).[21] The barrier for this dissociation is computed to be 22.16 kcal/mol at 100 °C. The dissociation of PPh_3 was confirmed by ^{31}P NMR studies (Figure S35) and HRMS studies (Figure S36). In the presence of methanol (**5**) and KO^{t}Bu, the dichloride species undergoes salt metathesis to form the Ru−methoxide species **7c**. The calculation of the energetics of the salt metathesis is not undertaken not only because this is typically a facile reaction but also because of the complex nature of the base (a cocktail of alkali−metal alkoxides in the reaction mixture) and the corresponding product salts (solvated or otherwise) involved.

The Ru−methoxide intermediate (**7c**) undergoes β−H elimination to give formaldehyde (**5′**) along with the formation of Ru−H species **9c** via **TS-8c**. This process is slightly uphill (ΔG_{100} = 7.56 kcal/mol) with a barrier of 17.70 kcal/mol (Figure 4). The formaldehyde (**5′**) can react with water either independently or in the presence of **9c**. While independent reaction of **5′** with one water leads to methanediol (**5″**) with a barrier of 33.14 kcal/mol, the corresponding reaction (**9c** → **TS-10c** → **11c**) in the presence of **9c** leads to **5″** coordinated **11c**, with a comparable barrier (32.25 kcal/mol) (Figure 4).

With an additional water molecule, while the corresponding barrier is much lower (11.77 kcal/mol) in the absence of **9c**, the reaction **9c** → **TS-10′c** → **11c** is almost barrierless in the presence of **9c**. Effectively, the presence of a second equivalent of water helps in lowering the barrier via a six-membered transition state for the conversion of formaldehyde (**5′**) to methanediol (**5″**) both in the presence and in the absence of **9c**. It is likely that **5″** is formed via the barrierless steps **9c** → **TS-10′c** → **11c** in the presence of an additional water molecule and remains coordinated to Ru in **11c**.

Subsequent σ-bond metathesis of the O−H bond in coordinated **5″** with the Ru−H bond of **11c** via **TS-12c** results in intermediate **13c** and the evolution of the first molecule of hydrogen, with a barrier of 23.85 kcal/mol and is an uphill process (ΔG_{100} = 7.81 kcal/mol). This is followed by a β-hydride elimination from the alkoxide coordinated to **13c**, leading to the formation of FA **6** (quantitatively detected in ^{1}H NMR) and the Ru−H species **9c** in a downhill process (ΔG_{100} = − 9.02 kcal/mol) with a barrier of $\Delta G^{\ddagger}_{100}$ = 11.40 kcal/mol (**TS-14c**). This lowest-energy (Figure 4) intermediate **9c** is detected by NMR as **9b′** (Figure S35). The resulting Ru−H species **9c** has two pathways available at its disposal. Apparently in a favorable path, the Ru−H bond in **9c** can undergo a σ-bond metathesis with the O−H of the methanol to generate back the Ru-methoxide species **7c** and the second molecule of hydrogen via **TS-18c** ($\Delta\Delta G^{\ddagger}_{100}$ = 18.64 kcal/mol) in an uphill reaction (ΔG_{100} = 3.10 kcal/mol). This completes the catalytic cycle for FA generation, which is an overall downhill process (ΔG_{100} = −0.33 kcal/mol) starting from equivalent amounts of methanol and water that also give rise to two equivalents of hydrogen.

Alternatively, liberation of second molecule of hydrogen and formation of Ru-formate **16c** via further σ-bond metathesis of the O−H of FA with the Ru−H bond in **9c** is likely to be difficult as it has a higher barrier (**TS-15c**, $\Delta\Delta G^{\ddagger}_{100}$ = 23.41 kcal/mol). This is in good agreement with the slight or no carbon dioxide observed during the reaction. However, when all the water is consumed, the FA cycle (**7c** → **TS-8c** → **9c** → **TS-10′c** → **11c** → **TS-12c** → **13c** → **TS-14c** → **9c** → **TS-18c** → **7c**) stops and then the cycle involving the formation of CO_2 (**7c** → **TS-8c** → **9c** → **TS-10′c** → **11c** → **TS-12c** → **13c** → **TS-14c** → **9c** → **TS-15c** → **16c** → **TS-17c** → **9c** → **TS-18c** → **7c**) may take over. This explains the observation of carbon dioxide at higher catalyst loadings (entries 8, 9, and 10, Table 3) and at lower concentrations of water (entries 11 and 12, Table 3).

The β-hydride elimination from the formate in **16c** via **TS-17c** ($\Delta\Delta G^{\ddagger}_{100}$ = 18.08 kcal/mol) with the concomitant release of carbon dioxide is a downhill reaction (ΔG_{100} = −14.75 kcal/mol). Finally, the Ru−H in intermediate **9c** undergoes σ-bond metathesis with the O−H of methanol to regenerate Ru-methoxide species **7c** via **TS-18c** along with the liberation of the third molecule of hydrogen. This is computed to be uphill (ΔG_{100} = 3.10 kcal/mol with a barrier of 18.63 kcal/mol. The overall process involving the generation of a mole of carbon dioxide and 3 moles of hydrogen from a mole each of methanol and water is downhill (ΔG_{100} = −17.00 kcal/mol). Single-point calculations at a higher level with Def2TZVP were also performed (Figure S34), and interestingly, the level of the calculation does not affect the trend of the result.

https://doi.org/10.1021/acscatal.2c05587
ACS Catal. 2023, 13, 3605−3617

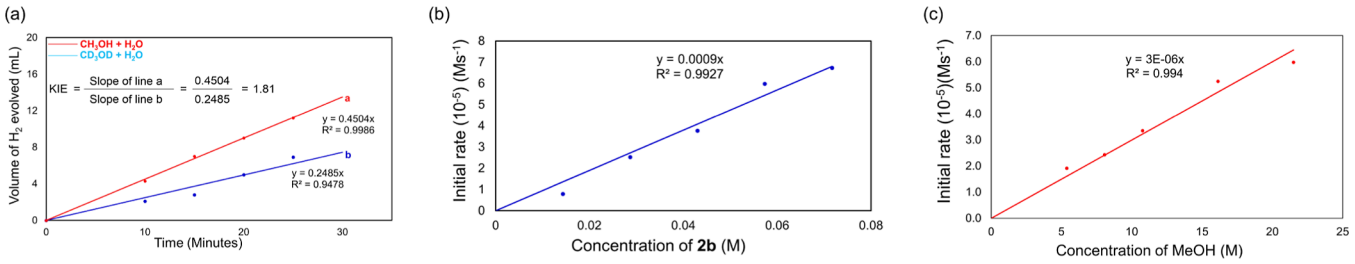

Figure 5. (a) Plot depicting the initial rate of gas evolution in the **2b** (0.8 mol %) catalyzed reaction of CH_3OH (13.92 mmol) with water (4.64 mmol) in the presence of KO^{t}Bu (6.96 mmol) at 100 °C and in the **2b** (0.8 mol %)-catalyzed reaction of CD_3OD (13.92 mmol) with water (4.64 mmol) in the presence of KO^{t}Bu (6.96 mmol) at 100 °C. Also see Figures S27 and S28. (b) Variation of initial rate of formation of FA with concentration of **2b** (reaction condition: methanol (0.433 mL, 10.71 mmol), D_2O (0.065 mL, 3.57 mmol), base (0.2 g, 1.78 mmol), and **2b** (0.2, 0.4, 0.6, 0.8, and 1 mol %) at 100 °C in a NMR tube). Also see Figure S25. (c) Variation of the initial rate of formation of FA with a concentration of methanol (reaction condition: methanol (0.108−0.433 mL, 2.67−10.71 mmol), D_2O (0.065 mL, 3.57 mmol), base (0.2 g, 1.78 mmol), and **2b** (0.8 mol %) at 100 °C in a NMR tube). Dioxane is used as a makeup solvent at lower concentrations of methanol. Also see Figure S26.

Either for the cycle involving the formation of a mole of FA and 2 moles of hydrogen or for the cycle that results in a mole of carbon dioxide and 3 moles of hydrogen, the σ-bond metathesis of the O−H bond in coordinated **5″** with the Ru−H bond of **11c** (**11c** → **TS-12c** → **13c**) appears to be the rate-determining step (RDS) with a barrier of 23.85 kcal/mol. Figure 4 clearly indicates **11c** and/or **9c** (formed via **TS-14c**) to be the resting states of the reaction, and not surprisingly, while **11b′**, the derivative of **11b**, is observed in HRMS analysis (Scheme 3 and Figure S36), the lowest energy intermediate **9c** is detected by NMR as **9b′** (Figure S35).

This is well-complemented by the deuterium-labeling studies that indicate a secondary kinetic isotope effect (KIE) where methanol C−H bond activation occurs as a part of the mechanism[12a] and is not a part of the RDS[12a] (Figure 5a), resulting in the H/D KIE value of 1.81. One should not be misled by the linear plot observed at initial time (Figure 5a) as the complete reaction profile is nonlinear (Figures S27 and S28). In fact, the reaction demonstrates a first-order dependence of rate on the concentration of methanol (Figure 5c and discussions vide infra).

The ratio of the TOF (8.00 mmol/48 h) of gas evolution for the **2b** catalyzed reaction of CH_3OH (13.92 mmol) with water (4.64 mmol) in the presence of KO^{t}Bu (6.96 mmol) at 100 °C to the corresponding TOF (3.78 mmol/48 h) of gas evolution starting from CD_3OD (13.92 mmol) and water (4.64 mmol) is 2.1 (eqs 1 vs 2, Scheme 4). This KIE of 2.1 very nicely correlates with the ratio (1.81) of the corresponding slopes of the initial rate of gas evolution (Figure 5a).

Only 38% retention of deuterium in FA upon use of CD_3OD + H_2O (Figure S29 and eq 2, Scheme 4) and its lack thereof while employing CH_3OH + D_2O (Figure S30 and eq 3, Scheme 4) suggests that while the steps (**7c** → **TS-8c** → **9c** → **TS-10c** → **11c**) and are reversible, the transformation (**11c** → **TS-12c** → **13c** → **TS-14c** → **9c**) is facile and irreversible. Similar results were obtained by Zheng[12b] and Singh[10] where they observed the participation of methanol C−H activation in the rate determining step. Not surprisingly, complete retention of deuterium was observed in FA in the reaction of CD_3OD + D_2O catalyzed by **2b** at 100 °C (Figures S31, S32 and eq 4, Scheme 4).

Apparently, the reaction is primarily homogeneous[25a−e] (see Page S53) and the major contributor to the observed reactivity was well-defined molecular pincer−Ru catalysts (eqs 1 vs 5, Scheme 4) with a minor contribution from heterogeneous Ru nanoparticles (NPs). Accordingly, the tiny amounts of black

Scheme 4. Control Experiments

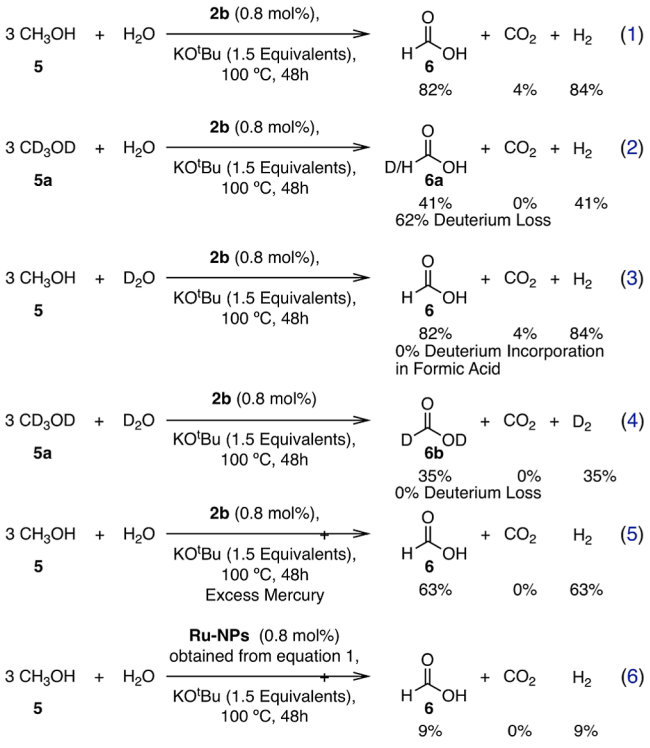

particles formed in the **2b** catalyzed reaction (entry 11, Table 3 and eq 1, Scheme 4) were analyzed by transmission electron microscopy (TEM) (Figure S24), separated, and used as a catalyst for methanol reforming under conditions identical as entry 11, Table 3. The poor reactivity (eq 6, Scheme 4) is suggestive of the fact that the formation of black Ru NPs is a deactivation step in the **2b**-catalyzed methanol reforming reaction.

Kinetic experiments were performed to determine the rate order of the reaction with respect to the concentration of the catalyst and methanol in a NMR tube. For the sake of ease of operation in a NMR tube, the reactions were performed using 0.5 equiv of KO^{t}Bu rather than 1.5 equiv. Using the initial rate method, it was found that the plots of the initial rate of formation of FA versus [**2b**] (Figures 5b and S25) and the initial rate of formation of FA versus [methanol] (Figures 5c and S26) is linear, which is indicative of first-order dependence on the concentrations of both **2b** and methanol.

https://doi.org/10.1021/acscatal.2c05587
ACS Catal. 2023, 13, 3605−3617

Scheme 5. On-Site Generation of Deuterium for Labeling Various Unsaturated Compounds

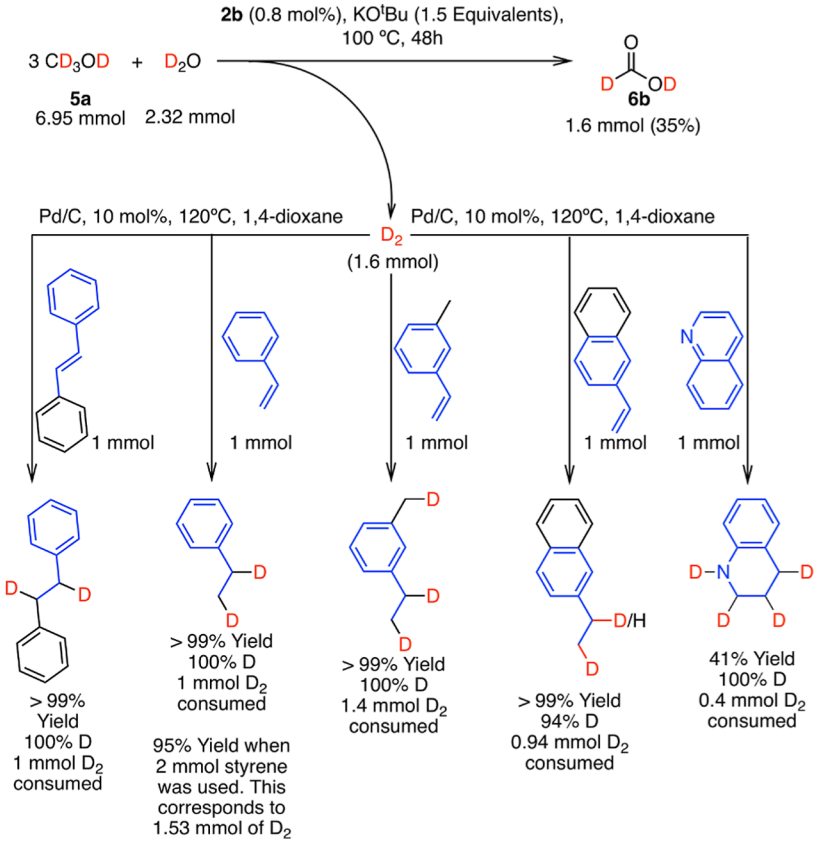

Steric bulk on the imine N could play a key role in deciding the barrier of the overall RDS involving the σ-bond metathesis of the O−H bond in coordinated **5″** with the Ru−H bond of **11** via **TS-12**. Considering the fact that the reaction is performed in water under an atmosphere of air, it is likely that a combination of steric factors and the relative stability toward moisture/air dictates the observed difference in reactivity of the various considered catalysts.

Obtaining the desired amount of deuterium for specialized experiments[25f] is often a challenge, not only owing to the fact that D_2 is less readily commercially available across all geographical locations but also because it is typically available in select expensive pack sizes. Taking into consideration, the immense applications of labeling organic compounds with hydrogen isotopes in numerous areas, from materials science to medicinal chemistry,[25f] the ability of the current catalytic system to produce pure hydrogen was put into valuable application toward the on-site synthesis of desired amounts of D_2 (Figure S33). Subsequent incorporation of the deuterium generated into various unsaturated molecules led to valuable compounds, including but not limited to reduced quinoline derivatives, which are key structural features of many natural and unnatural compounds with important biological properties such as antibacterial, antifungal, and anticancer activity (Scheme 5).[25g] The yields of hydrogen/deuterium calculated by measuring the volume of gas evolved are very consistent and comparable to the corresponding yields of reduced products obtained (see footnote i, Table 3 and the total deuterium incorporated in ethyl benzene and 1-ethyl-3-methylbenzene, Scheme 5).

CONCLUSIONS

NNN pincer−ruthenium complexes of the type (^{R2}NNN)-$RuCl_2(CH_3CN)$ based on *bis*(imino)pyridine ligands have been synthesized and characterized. Apart from their phosphine and carbonyl counterparts, these pincer ruthenium acetonitrile complexes were tested for the value-addition of methanol via its reforming in the presence of a base. In comparison with the considered catalysts, the best efficiency was observed with (^{Cy2}NNN)$RuCl_2(PPh_3)$. KO^{t}Bu (0.5 equiv with respect to water) was found to give superior results at temperatures as low as 100 °C among the bases screened. For a mixture of methanol and water in a 2:1 ratio (^{Cy2}NNN)-$RuCl_2(PPh_3)$ (0.2 mol %) gave a yield of up to 81% each of hydrogen and FA at 100% selectivity in the presence of KO^{t}Bu (1.5 equiv with respect to water) at 100 °C. However, under identical conditions, a higher loading of (^{Cy2}NNN)-$RuCl_2(PPh_3)$ (2 mol %) gave up to 90% of hydrogen and 73% of FA at 80% selectivity. In contrast, use of a 3:1 methanol/water mixture resulted in good yields (84%) of hydrogen with 82% FA at 95% selectivity at a 0.8 mol % loading of (^{Cy2}NNN)$RuCl_2(PPh_3)$. The yields of hydrogen/deuterium calculated by measuring the volume of gas evolved are very consistent and comparable to the yields of products obtained by using them for reducing the corresponding unsaturated compounds.

Valuable information was obtained from detailed mechanistic studies. Evidence for the homogeneous nature of the reaction involving well-defined molecular catalysts was obtained from kinetic studies that demonstrated a first-order dependence of rate on the concentrations of both (^{Cy2}NNN)-$RuCl_2(PPh_3)$ and methanol. Deuterium-labeling studies were

https://doi.org/10.1021/acscatal.2c05587
ACS Catal. 2023, 13, 3605−3617

indicative of an average KIE of 1.96 that points to a secondary KIE where methanol C−H bond activation occurs as a part of the mechanism but not as a part of the RDS. This is very well complemented by DFT studies that compute that either for the cycle leading to FA and 2 mol of hydrogen or for the cycle that results in carbon dioxide and 3 moles of hydrogen, the σ-bond metathesis leading to the elimination of the first molecule of hydrogen is the RDS. The unprecedented selectivity toward FA in these pincer−ruthenium catalyzed methanol reforming stems from the choice of the Ru−H bond in (^{Cy2}NNN)RuCl-(H) to undergo a σ-bond metathesis either with the O−H of methanol (that completes the FA cycle) or with the O−H of FA that leads to carbon dioxide. Its preference for the former is mainly dictated by kinetics, which is more favored by 4.58 kcal/mol. We report a powerful catalytic system that comprises of an NNN pincer-ruthenium phosphine catalyst based on *bis*(imino)pyridine ligand for the high yield transformation of a mole of methanol and water to 2 moles of hydrogen and a mole of FA at unprecedented selectivity at a temperature as low 100 °C. This could open up exciting avenues for the reforming of methanol into clean-burning hydrogen and high-value FA.

EXPERIMENTAL SECTION

General Procedure and Materials. All manipulations were carried out under purified Ar using a standard double manifold or a glove box. The solvents such as tetrahydrofuran, hexane, and toluene were dried via double distillation over Na/benzophenone prior to the experiment.[26] Methanol was dried and distilled under argon according to the literature procedure.[26] All other chemicals, such as pyridine-2,6-dicarboxylic acid, $[RuCl_2(p\text{-cymene})]_2$, D_2O, and CD_3OD, were purchased from MERCK or Sigma-Aldrich and used as such. All catalytic reactions were set up under an argon atmosphere using dried glassware. The ligands **4a−c** and complexes **1a−f** and **2a−f** were prepared according to the literature procedure.[21−24,27]

Physical Measurements. ^{1}H, ^{2}H, ^{13}C{H}, ^{31}P, and ^{19}F NMR were recorded on a Bruker ASCEND 600 operating at 600 MHz for ^{1}H, 150 MHz for ^{13}C{H}, 564 MHz for ^{31}P, and 565 MHz for ^{19}F or on a Bruker AVANCE 400 operating at 400 MHz for ^{1}H, 100 MHz for ^{13}C{H}, 376 MHz for ^{31}P, and 377 MHz for ^{19}F or on a Bruker AVANCE 500 operating at 500 MHz for ^{1}H, 125 MHz for ^{13}C{H}, 470 MHz for ^{31}P, and 471 MHz for ^{19}F. Chemical shifts (δ) are reported in ppm, spin−spin coupling constants (J) are expressed in Hz, and other data are reported as follows: s = singlet, d = doublet, t = triplet, m = multiplet, q = quartet, and br s = broad singlet. HRMS measurements were done using an Agilent Accurate-Mass Q-TOF ESI−MS 6520. X-ray crystallographic data were collected on a Bruker D8 Venture single-crystal X-ray diffractometer with graphite-monochromated Mo Kα radiation. The data refinement and cell reductions were carried out. The crystal structures were solved by SHELXL[28a] and refined by full-matrix least squares on F^2 using SHELXL.[28b] GC analyses were performed on an Agilent 7820-GC instrument fitted with a Agilent Front SS7 inlet N2 HP-PLOT Q column (30 m length × 530 μm × 40 μm) using the following method: Agilent 7820-GC back detector; TCD starting temperature: 40 °C; time at starting temp: 0 min; ramp: 40 °C/min up to 250 °C with a hold time = 5 min; flow rate (carrier): 25 mL/min (N2); split ratio: 195; inlet temperature: 40 °C; and detector temperature: TCD: 250 °C, FID: 250 °C.

General Procedure for the Synthesis of (^{R2}NNN)-$RuCl_2(CH_3CN)$ Complexes (3a; R = Cy, 3b; R = ^{i}Pr and 3c; R = Ph). The complexes **3a** were prepared by the reaction of corresponding ligands **4a** (0.100 g, 0.393 mmol) with $[RuCl_2(p\text{-cymene})]_2$ (0.120 g, 0.196 mmol), using acetonitrile as the solvent and stirring overnight under reflux conditions. The solvent was evaporated under reduced pressure, and the dark brown solid (**3a**) was washed with diethyl ether (3 × 3 mL). The residue was dried under a vacuum and **3a** isolated as a black solid with a 64% yield (0.128 g). A similar procedure was followed for the synthesis of **3a−c**.

(^{Cy2}NNN)$RuCl_2(CH_3CN)$ (3a). (0.128 g) 64% yield. NMR analysis shows the presence of two isomers (cis and trans) in a 1:2 ratio. ^{1}H NMR (600 MHz, $CDCl_3$): δ 8.57 (s, 2H), 8.34 (s, 4H), 8.02−7.95 (m, 2H), 7.79 (s, 1H), 7.59 (d, J = 7.8 Hz, 4H), 7.43 (t, J = 7.7 Hz, 2H), 3.96 (ddt, J = 11.3, 8.0, 3.3 Hz, 6H), 2.91 (s, 3H), 2.83 (s, 6H), 2.26−2.28 (m, J = 8.4, 4.3 Hz, 9H), 2.14−2.17 (m, 6H), 1.99−1.93 (m, 12H), 1.91−1.84 (m, 14H), 1.47−1.40 (m, 12H), 1.25 (d, J = 6.9 Hz, 7H). ^{13}C{H} NMR (151 MHz, $CDCl_3$): δ 161.91, 159.47, 128.99, 127.82, 126.28, 122.35, 72.54, 33.52, 26.07, 25.93, 25.52, 25.26, 24.10, 23.57, 4.90. HRMS (ESI): m/z calculated for $[\mathbf{3a} - Cl]^+ = [C_{21}H_{30}ClN_4Ru]^+$, 475.1202; found, 475.1352; m/z calcd for $[M - Cl + CH_3CN]^+ = [C_{23}H_{33}ClN_5Ru]^+$, 516.1468; found, 516.1628.

(^{iPr2}NNN)$RuCl_2(CH_3CN)$ (3b). (0.117 g, black solid) 81% yield. NMR analysis shows the presence of two isomers (cis and trans) in a 1:2 ratio. ^{1}H NMR (600 MHz, $CDCl_3$): δ 8.56 (s, 2H), 8.37 (s, 4H), 7.96 (d, J = 7.4 Hz, 2H), 7.78 (t, J = 7.1 Hz, 1H), 7.60 (d, J = 7.8 Hz, 4H), 7.44 (t, J = 7.8 Hz, 2H), 4.39−4.30 (m, 6H), 2.91 (s, 3H), 2.84 (s, 6H), 1.61 (d, J = 6.5 Hz, 22H), 1.56 (d, J = 5.0 Hz, 14H). ^{13}C NMR (151 MHz, $CDCl_3$); δ 163.26, 161.83, 160.60, 159.55, 134.01, 129.00, 128.08, 125.42, 122.41, 77.29, 77.08, 76.87, 65.29, 64.63, 23.19, 22.94, 22.91, 5.17, 4.79. HRMS (ESI): m/z calculated for $[\mathbf{3b} - Cl - CH_3CN]^+ = [C_{13}H_{19}ClN_3Ru]^+$, 354.0311; found, 354.0304; m/z calcd for $[\mathbf{3b} - Cl]^+ = [C_{15}H_{22}ClN_4Ru]^+$, 395.0576; found, 395.0575; m/z calcd for $[\mathbf{3b} - Cl + CH_3CN]^+ = [C_{17}H_{25}ClN_5Ru]^+$, 436.0842; found, 436.0845.

(^{Ph2}NNN)$RuCl_2(CH_3CN)$ (3c). (0.116 g, purple solid) 69% yield. ^{1}H NMR (400 MHz, $CDCl_3$): δ 8.38 (s, 2H), 7.73 (d, J = 7.9 Hz, 2H), 7.65 (d, J = 8.4 Hz, 4H), 7.48 (t, J = 7.9 Hz, 1H), 7.34 (dd, J = 11.9, 7.3 Hz, 6H), 2.31 (s, 3H). ^{13}C{H} NMR (151 MHz, $CDCl_3$): δ 160.30, 154.78, 150.96, 137.50, 129.42, 127.07, 123.43, 121.33, 77.37, 77.16, 76.95, 1.16. HRMS (ESI): m/z calcd for $[\mathbf{3c} - Cl - CH_3CN]^+ = [C_{19}H_{15}ClN_3Ru]^+$, 421.9998; found, 421.9986; m/z calcd for $[\mathbf{3c} - Cl]^+ = [C_{21}H_{18}ClN_4Ru]^+$, 463.0263; found, 463.0261; m/z calcd for $[\mathbf{3c} - Cl + CH_3CN]^+ = [C_{23}H_{21}ClN_5Ru]^+$, 504.0529; found, 504.0525.

General Procedure for the Aqueous Methanol Reforming Reaction. In a 5 mL pear-shaped vessel attached to a condenser, KO^{t}Bu (0.390 g, 3.48 mmol) and **2b** (0.04−0.8 mol %; 0.0007−0.0136 g; 0.9−18.5 μmol) were added inside the glove box. This was followed by the addition of dry methanol (**4**) (0.188 mL, 4.635 mmol) or (0.282 mL, 6.951 mmol) and distilled water (0.042 mL, 2.317 mmol) under an Ar atmosphere. The mixture was heated in a preheated oil bath at 100 °C, and the gas evolved was quantified by the water displacement method, and the composition of the gas generated was analyzed by GC (see Supporting Information for the details). The reaction was run till no more evolution of

https://doi.org/10.1021/acscatal.2c05587
ACS Catal. 2023, 13, 3605−3617

gas was observed (typically 48 h) and was then cooled down to room temperature. An aliquot (10 mg approx.) was withdrawn from the reaction mixture, and the yield of the FA was determined by ^{1}H NMR using D_2O as the solvent and sodium acetate (known amount added in the NMR tube) as a standard.

General Procedure for the On-Site Generation of Deuterium and Its Incorporation in Unsaturated Substrates. In a 5 mL pear-shaped vessel (**A**) attached to a condenser, KO^{t}Bu (0.390 g, 3.48 mmol), **2b** (0.8 mol %; 0.0136 g; 18.5 μmol), and anhydrous methanol-d_4(**5a**) (0.282 mL, 6.951 mmol) were added inside the glove box. This was followed by the addition of D_2O (0.042 mL, 2.317 mmol) under an Ar atmosphere. On the other hand, Pd/C (10 mol %; 0.0106 g; 0.1 mmol), unsaturated substrate (1 mmol), and 1,4-dioxane (0.5 mL) were added to a 30 mL bomb vessel **B** under an Ar atmosphere. The deuterium gas generated in the flask **A** at 100 °C was fed to bomb vessel **B** at 120 °C for 48 h and then cooled down to room temperature. An aliquot (10 mg approx.) was withdrawn from the reaction mixture of **A**, and the NMR yield of the FA-d_2 was determined by ^{2}H NMR using H_2O as the solvent and D_2O (known amount added in the NMR tube) as an internal standard. The ^{1}H NMR analysis was also done to check the formation of FA (if any). An aliquot (10 mg approx.) was withdrawn from the reaction mixture of **B**, and the NMR yield of the deuterated product was determined by ^{1}H NMR using $CDCl_3$ as the solvent and toluene (known amount added in the flask) as the internal standard. The ^{2}H NMR analysis was also done to check the deuterium incorporation in the product.

General procedure of the kinetic studies performed for the 2b catalyzed transformation of methanol to FA.

Variation of Catalyst Concentration. In a J-Young Teflon valve NMR tube, KO^{t}Bu (0.200 g, 1.79 mmol) and **2b** (0.2−1 mol %; 0.0050−0.0261 g; 7.14−35.7 μmol) were added inside the glove box. This was followed by the addition of dry methanol (**5**) (0.433 mL, 10.71 mmol) and D_2O (0.065 mL, 3.57 mmol) under an Ar atmosphere. The tube was heated in a preheated oil bath at 100 °C. ^{1}H NMR of the reaction mixture was recorded at different time intervals using sodium acetate as a standard.

Variation of MeOH Concentration. In a J-Young Teflon valve NMR tube, KO^{t}Bu (0.200 g, 1.79 mmol) and **2b** (0.8 mol %; 0.0209 g; 28.56 μmol) were added inside the glove box. This was followed by the addition of dry methanol (**5**) (0.433−0.108 mL, 10.71−2.67 mmol) and D_2O (0.065 mL, 3.57 mmol) under an Ar atmosphere. Dioxane was used as a make-up solvent at lower concentrations of methanol. The tube was heated in a preheated oil bath at 100 °C. ^{1}H NMR of the reaction mixture was recorded at different time intervals using sodium acetate as a standard.

Computational Details. The geometries of all the considered complexes were fully optimized employing the DFT(PBEPBE)[29] method on the Gaussian-09 package.[30] The Def2SVP[31] basis set with a polarization function was used for the metal (Ru) and nonmetal atoms. The empirical dispersion-GD3 was used in all molecular geometry optimization and energy computations. The transition states were located using the synchronous transit-guided quasi-Newton (QST2) method. The method and basis set were selected on the basis of previous reports on pincer complexes.[23] Frequency calculations were also done to differentiate minima structures or transition states on the potential energy surface. Single point calculations were performed to calculate the relative free energy values at 100 °C. Single-point calculations were also performed at a higher level with Def2TZVP.

■ ASSOCIATED CONTENT

Data Availability Statement

These data can be obtained free of charge via www.ccdc.cam.ac.uk/data_request/cif, or by emailing data_request@ccdc.cam.ac.uk, or by contacting The Cambridge Crystallographic Data Centre, 12 Union Road, Cambridge CB2 1EZ, UK; fax: +44 1223 336033.

Supporting Information

The Supporting Information is available free of charge at https://pubs.acs.org/doi/10.1021/acscatal.2c05587.

Detailed experimental procedure, NMR, X-ray crystallographic parameters, IR, TEM, HRMS analysis, computational details, and Cartesian coordinates (PDF)

CCDC 2111523 contains the supplementary crystallographic data (CIF)

CCDC 2111524 contains the supplementary crystallographic data (CIF)

■ AUTHOR INFORMATION

Corresponding Author

Akshai Kumar − *Department of Chemistry, Centre for Nanotechnology, and Jyoti and Bhupat Mehta School of Health Sciences and Technology, Indian Institute of Technology Guwahati, Guwahati, Assam 781039, India;* orcid.org/0000-0002-3911-3630; Email: akshaikumar@iitg.ac.in

Authors

Vinay Arora − *Department of Chemistry, Indian Institute of Technology Guwahati, Guwahati, Assam 781039, India;* orcid.org/0000-0003-0356-4680

Eileen Yasmin − *Department of Chemistry, Indian Institute of Technology Guwahati, Guwahati, Assam 781039, India*

Niharika Tanwar − *Centre for Nanotechnology, Indian Institute of Technology Guwahati, Guwahati, Assam 781039, India*

Venkatesha R. Hathwar − *School of Physical and Applied Sciences, Goa University, Goa 403206, India;* orcid.org/0000-0001-9438-417X

Tushar Wagh − *ChemDist Group of Companies, Pune, Maharashtra 411026, India*

Sunil Dhole − *ChemDist Group of Companies, Pune, Maharashtra 411026, India*

Complete contact information is available at: https://pubs.acs.org/10.1021/acscatal.2c05587

Author Contributions

V.A. and E.Y. carried out all of the experiments with the assistance for a few from N.T. While V.R.H. assisted in crystallographic analysis, S.D. and T.W. were instrumental in providing valuable intellectual inputs. A.K. conceptualized the project and wrote the manuscript.

Funding

Science and Engineering Research Board (SERB), Department of Science and Technology. Scheme for Transformational and Advanced Research in Sciences (STARS), Ministry of Human Resource Development, Implemented by Indian Institute of

Science, Bangalore. Ministry of Electronics and Information Technology. Indian Council of Medical Research.

Notes

The authors declare no competing financial interest.

■ ACKNOWLEDGMENTS

A.K. is grateful for the grants received from the Science and Engineering Research Board (grant no. DST-SERB CRG/2022/002354). A.K. acknowledges the Scheme for Transformational and Advanced Research in Sciences, Ministry of Education, implemented by the Indian Institute of Science (IISc), Bangalore (grant no. STARS/APR2019/CS/629/FS). The funds received from the Ministry of Electronics and Information Technology via the INUP-I2I program (5(1)/2021-NANO) and the SWASTHA COE (5(1)/2022-NANO) are gratefully acknowledged. Thanks are also due for the financial support from the Indian Council of Medical Research, New Delhi (5/3/8/20/2019-ITR). The DST-FIST program, NECBH-IITG, the Department of Chemistry at IITG, and CIF-IITG are acknowledged for various instrumental facilities.

■ ABBREVIATIONS

TON, turnover number; TOF, turnover frequency; TOs/h, turnovers per hour; THF, tetrahydrofuran; RDS, rate-determining step

■ REFERENCES

(1) (a) Ragauskas, A. J.; Williams, C. K.; Davison, B. H.; Britovsek, G.; Cairney, J.; Eckert, C. A.; Frederick, W. J.; Hallett, J. P.; Leak, D. J.; Liotta, C. L.; Mielenz, J. R.; Murphy, R.; Templer, R.; Tschaplinski, T. The Path Forward for Biofuels and Biomaterials. *Science* **2006**, *311*, 484−489. (b) Kumar, A.; Bhatti, T. M.; Goldman, A. S. Dehydrogenation of Alkanes and Aliphatic Groups by Pincer-Ligated Metal Complexes. *Chem. Rev.* **2017**, *117*, 12357−12384.

(2) Rahman, A.; Farrok, O.; Haque, M. M. Environmental impact of renewable energy source based electrical power plants: Solar, wind, hydroelectric, biomass, geothermal, tidal, ocean, and osmotic. *Renewable Sustainable Energy Rev.* **2022**, *161*, 112279.

(3) (a) Kumar, A.; Daw, P.; Milstein, D. Homogeneous Catalysis for Sustainable Energy: Hydrogen and Methanol Economies, Fuels from Biomass, and Related Topics. *Chem. Rev.* **2022**, *122*, 385−441. (b) Yadav, V.; Sivakumar, G.; Gupta, V.; Balaraman, E. Recent Advances in Liquid Organic Hydrogen Carriers: An Alcohol-Based Hydrogen Economy. *ACS Catal.* **2021**, *11*, 14712−14726. (c) Das, K.; Kumar, A. Alkane dehydrogenation reactions catalyzed by pincer-metal complexes. In *Advances in Organometallic Chemistry*; Pérez, P. J., Ed.; Academic Press, 2019; Vol. *72*, Chapter 1, pp 1−57. (d) Satyapal, S.; Petrovic, J.; Read, C.; Thomas, G.; Ordaz, G. The U.S. Department of Energy's National Hydrogen Storage Project: Progress towards meeting hydrogen-powered vehicle requirements. *Catal. Today* **2007**, *120*, 246−256. (e) Singh, S.; Jain, S.; Ps, P.; Tiwari, A. K.; Nouni, M. R.; Pandey, J. K.; Goel, S. Hydrogen: A sustainable fuel for future of the transport sector. *Renew. Sustain. Energy Rev.* **2015**, *51*, 623−633. (f) El-Shafie, M.; Kambara, S.; Hayakawa, Y. Hydrogen production technologies overview. *J. Power Energy Eng.* **2019**, *07*, 107−154. (g) Abdin, Z.; Zafaranloo, A.; Rafiee, A.; Mérida, W.; Lipiński, W.; Khalilpour, K. R. Hydrogen as an energy vector. *Renew. Sustain. Energy Rev.* **2020**, *120*, 109620. (h) Dincer, I. Green methods for hydrogen production. *Int. J. Hydrogen Energy* **2012**, *37*, 1954−1971. (i) Qureshi, F.; Yusuf, M.; Kamyab, H.; Vo, D.-V. N.; Chelliapan, S.; Joo, S.-W.; Vasseghian, Y. Latest eco-friendly avenues on hydrogen production towards a circular bioeconomy: Currents challenges, innovative insights, and future perspectives. *Renew. Sustain. Energy Rev.* **2022**, *168*, 112916. (j) Kumar, S.; Lim, H. An overview of water electrolysis technologies for green hydrogen production. *Energy Rep.* **2022**, *8*, 13793−13813. (k) Temiz, M.; Dincer, I. Development and assessment of an onshore wind and concentrated solar based power, heat, cooling and hydrogen energy system for remote communities. *J. Clean. Prod.* **2022**, *374*, 134067. (l) Temiz, M.; Dincer, I. Development of solar and wind based hydrogen energy systems for sustainable communities. *Energy Convers. Manag.* **2022**, *269*, 116090. (m) Xu, X.; Zhou, Q.; Yu, D. The future of hydrogen energy: Bio-hydrogen production technology. *Int. J. Hydrogen Energy* **2022**, *47*, 33677−33698. (n) El-Emam, R. S.; Özcan, H. Comprehensive review on the techno-economics of sustainable large-scale clean hydrogen production. *J. Clean. Prod.* **2019**, *220*, 593−609. (o) Mancera, J. J. C.; Manzano, F. S.; Andújar, J. M.; López, E.; Isorna, F. Sun, heat and electricity. A comprehensive study of non-pollutant alternatives to produce green hydrogen. *Int. J. Energy Res.* **2022**, *46*, 17999−18028. (p) Sadaghiani, M. S.; Mehrpooya, M. Introducing and energy analysis of a novel cryogenic hydrogen liquefaction process configuration. *Int. J. Hydrogen Energy* **2017**, *42*, 6033−6050. (q) Sreedhar, I.; Kamani, K. M.; Kamani, B. M.; Reddy, B. M.; Venugopal, A., A Bird's Eye view on process and engineering aspects of hydrogen storage. **2018**, *91*, 838-860; DOI: 10.1016/j.rser.2018.04.028 (r) Green, M. A. Hydrogen safety issues compared to safety issues with methane and propane. In *AIP conference Proceedings 2006 American Institute of Physics*; American Institute of Physics, 2006, pp 319−326. (s) Li, H.; Cao, X.; Liu, Y.; Shao, Y.; Nan, Z.; Teng, L.; Peng, W.; Bian, J. Safety of hydrogen storage and transportation: An overview on mechanisms, techniques, and challenges. *Energy Rep.* **2022**, *8*, 6258−6269. (t) Sinigaglia, T.; Lewiski, F.; Martins, M. E. S.; Siluk, J. C. M. Production, storage, fuel stations of hydrogen and its utilization in automotive applications-a review. *Int. J. Hydrogen Energy* **2017**, *42*, 24597−24611. (u) Ren, J.; Musyoka, N. M.; Langmi, H. W.; Mathe, M.; Liao, S. Current research trends and perspectives on materials-based hydrogen storage solutions: A critical review. *Int. J. Hydrogen Energy* **2017**, *42*, 289−311. (v) Modisha, P. M.; Ouma, C. N. M.; Garidzirai, R.; Wasserscheid, P.; Bessarabov, D. The Prospect of Hydrogen Storage Using Liquid Organic Hydrogen Carriers. *Energy Fuels* **2019**, *33*, 2778−2796. (w) Gianotti, E.; Taillades-Jacquin, M.; Rozière, J.; Jones, D. J. High-Purity Hydrogen Generation via Dehydrogenation of Organic Carriers: A Review on the Catalytic Process. *ACS Catal.* **2018**, *8*, 4660−4680. (x) Hietala, J.; Vuori, A.; Johnsson, P.; Pollari, I.; Reutemann, W.; Kieczka, H. Formic Acid. In *Ullmann's Encyclopedia of Industrial Chemistry*; Wiley-VCH Verlag GmbH & Co. KGaA: Weinheim, 2016, pp 1−22. (y) Zhai, S.; Jiang, S.; Liu, C.; Li, Z.; Yu, T.; Sun, L.; Ren, G.; Deng, W. Liquid Sunshine: Formic Acid. *J. Phys. Chem. Lett.* **2022**, *13*, 8586−8600. (z) Eppinger, J.; Huang, K.-W. Formic Acid as a Hydrogen Energy Carrier. *ACS Energy Lett.* **2017**, *2*, 188−195.

(4) (a) Nielsen, M.; Alberico, E.; Baumann, W.; Drexler, H. J.; Junge, H.; Gladiali, S.; Beller, M. Low-temperature aqueous-phase methanol dehydrogenation to hydrogen and carbon dioxide. *Nature* **2013**, *495*, 85−89. (b) Lei, M.; Pan, Y.; Ma, X. The Nature of Hydrogen Production from Aqueous-Phase Methanol Dehydrogenation with Ruthenium Pincer Complexes Under Mild Conditions. *Eur. J. Inorg. Chem.* **2015**, *2015*, 794−803.

(5) Rodríguez-Lugo, R. E.; Trincado, M.; Vogt, M.; Tewes, F.; Santiso-Quinones, G.; Grützmacher, H. A homogeneous transition metal complex for clean hydrogen production from methanol-water mixtures. *Nat. Chem.* **2013**, *5*, 342.

(6) Govindarajan, N.; Sinha, V.; Trincado, M.; Grützmacher, H.; Meijer, E. J.; Bruin, B. An In-Depth Mechanistic Study of Ru-Catalysed Aqueous Methanol Dehydrogenation and Prospects for Future Catalyst Design. *ChemCatChem* **2020**, *12*, 2610−2621.

(7) Sinha, V.; Govindarajan, N.; de Bruin, B.; Meijer, E. J. How Solvent Affects C−H Activation and Hydrogen Production Pathways in Homogeneous Ru-Catalyzed Methanol Dehydrogenation Reactions. *ACS Catal.* **2018**, *8*, 6908−6913.

(8) Monney, A.; Barsch, E.; Sponholz, P.; Junge, H.; Ludwig, R.; Beller, M. Base-free hydrogen generation from methanol using a bi-catalytic system. *Chem. Commun.* **2014**, *50*, 707−709.

https://doi.org/10.1021/acscatal.2c05587
ACS Catal. 2023, 13, 3605−3617

(9) Hu, P.; Diskin-Posner, Y.; Ben-David, Y.; Milstein, D. Reusable Homogeneous Catalytic System for Hydrogen Production from Methanol and Water. *ACS Catal.* **2014**, *4*, 2649−2652.
(10) Awasthi, M. K.; Rai, R. K.; Behrens, S.; Singh, S. K. Low-temperature hydrogen production from methanol over a ruthenium catalyst in water. *Catal. Sci. Technol.* **2021**, *11*, 136−142.
(11) Luo, J.; Kar, S.; Rauch, M.; Montag, M.; Ben-David, Y.; Milstein, D. Efficient Base-Free Aqueous Reforming of Methanol Homogeneously Catalyzed by Ruthenium Exhibiting a Remarkable Acceleration by Added Catalytic Thiol. *J. Am. Chem. Soc.* **2021**, *143*, 17284−17291.
(12) (a) Simmons, E. M.; Hartwig, J. F. On the Interpretation of Deuterium Kinetic Isotope Effects in C−H Bond Functionalizations by Transition-Metal Complexes. *Angew. Chem., Int. Ed.* **2012**, *51*, 3066−3072. (b) Wang, Q.; Lan, J.; Liang, R.; Xia, Y.; Qin, L.; Chung, L. W.; Zheng, Z. New Tricks for an Old Dog: Grubbs Catalysts Enable Efficient Hydrogen Production from Aqueous-Phase Methanol Reforming. *ACS Catal.* **2022**, *12*, 2212−2222.
(13) Morton, D.; Cole-Hamilton, D. J. Rapid thermal hydrogen production from alcohols catalysed by [Rh(2,2′-bipyridyl)2]Cl. *J. Chem. Soc., Chem. Commun.* **1987**, *4*, 248−249.
(14) Zhan, Y.-L.; Shen, Y.-B.; Li, S.-P.; Yue, B.-H.; Zhou, X.-C. Hydrogen generation from methanol reforming under unprecedented mild conditions. *Chin. Chem. Lett.* **2017**, *28*, 1353−1357.
(15) Campos, J.; Sharninghausen, L. S.; Manas, M. G.; Crabtree, R. H. Methanol Dehydrogenation by Iridium N-Heterocyclic Carbene Complexes. *Inorg. Chem.* **2015**, *54*, 5079−5084.
(16) Fujita, K.-i.; Kawahara, R.; Aikawa, T.; Yamaguchi, R. Hydrogen Production from a Methanol−Water Solution Catalyzed by an Anionic Iridium Complex Bearing a Functional Bipyridonate Ligand under Weakly Basic Conditions. *Angew. Chem., Int. Ed.* **2015**, *54*, 9057−9060.
(17) Prichatz, C.; Alberico, E.; Baumann, W.; Junge, H.; Beller, M. Iridium−PNP Pincer Complexes for Methanol Dehydrogenation at Low Base Concentration. *ChemCatChem* **2017**, *9*, 1891−1896.
(18) Alberico, E.; Sponholz, P.; Cordes, C.; Nielsen, M.; Drexler, H.-J.; Baumann, W.; Junge, H.; Beller, M. Selective Hydrogen Production from Methanol with a Defined Iron Pincer Catalyst under Mild Conditions. *Angew. Chem., Int. Ed.* **2013**, *52*, 14162−14166.
(19) Bielinski, E. A.; Förster, M.; Zhang, Y.; Bernskoetter, W. H.; Hazari, N.; Holthausen, M. C. Base-Free Methanol Dehydrogenation Using a Pincer-Supported Iron Compound and Lewis Acid Co-catalyst. *ACS Catal.* **2015**, *5*, 2404−2415.
(20) Andérez-Fernández, M.; Vogt, L. K.; Fischer, S.; Zhou, W.; Jiao, H.; Garbe, M.; Elangovan, S.; Junge, K.; Junge, H.; Ludwig, R.; Beller, M. A Stable Manganese Pincer Catalyst for the Selective Dehydrogenation of Methanol. *Angew. Chem., Int. Ed.* **2017**, *129*, 574−577.
(21) Das, K.; Nandi, P. G.; Islam, K.; Srivastava, H. K.; Kumar, A. N−Alkylation of Amines Catalyzed by a Ruthenium−Pincer Complex in the Presence of in situ Generated Sodium Alkoxide. *Eur. J. Org. Chem.* **2019**, *2019*, 6855−6866.
(22) Dutta, M.; Das, K.; Prathapa, S. J.; Srivastava, H. K.; Kumar, A. Selective and high yield transformation of glycerol to lactic acid using NNN pincer ruthenium catalysts. *Chem. Commun.* **2020**, *56*, 9886−9889.
(23) (a) Das, K.; Yasmin, E.; Das, B.; Srivastava, H. K.; Kumar, A. Phosphine-free pincer-ruthenium catalyzed biofuel production: high rates, yields and turnovers of solventless alcohol alkylation. *Catal. Sci. Technol.* **2020**, *10*, 8347−8358. (b) Das, K.; Kathuria, L. K.; Jasra, R. V.; Dhole, S.; Kumar, A. Microwave Assisted Pincer-Ruthenium Catalyzed Guerbet Reaction for the Upgradation of Bio-Ethanol to Bio-Butanol. *Catal. Sci. Technol.* **2023**, DOI: 10.1039/D3CY00079F.
(24) (a) Das, K.; Dutta, M.; Das, B.; Srivastava, H. K.; Kumar, A. Efficient Pincer-Ruthenium Catalysts for Kharasch Addition of Carbon Tetrachloride to Styrene. *Adv. Synth. Catal.* **2019**, *361*, 2965−2980. (b) Das, K.; Yasmin, E.; Kumar, A. Pincer-Ruthenium Catalyzed Oxygen Mediated Dehydrative Etherification of Alcohols and Ortho-Alkylation of Phenols. *Adv. Synth. Catal.* **2022**, *364*, 3895−3909.
(25) (a) Narjinari, H.; Tanwar, N.; Kathuria, L.; Jasra, R. V.; Kumar, A. Guerbet-type β-alkylation of secondary alcohols catalyzed by chromium chloride and its corresponding NNN pincer complex. *Catal. Sci. Technol.* **2022**, *12*, 4753−4762. (b) Nandi, P. G.; Kumar, P.; Kumar, A. Ligand-free Guerbet-type reactions in air catalyzed by in situ formed complexes of base metal salt cobaltous chloride. *Catal. Sci. Technol.* **2022**, *12*, 1100−1108. (c) Arora, V.; Narjinari, H.; Kumar, A. Pincer-Nickel Catalyzed Selective Guerbet-Type Reactions. *Organometallics* **2021**, *40*, 2870−2880. (d) Arora, V.; Dutta, M.; Das, K.; Das, B.; Srivastava, H. K.; Kumar, A. Solvent-Free N-Alkylation and Dehydrogenative Coupling Catalyzed by a Highly Active Pincer-Nickel Complex. *Organometallics* **2020**, *39*, 2162−2176. (e) Nandi, P. G.; Thombare, P.; Prathapa, S. J.; Kumar, A. Pincer-Cobalt-Catalyzed Guerbet-Type β-Alkylation of Alcohols in Air under Microwave Conditions. *Organometallics* **2022**, *41*, 3387−3398. (f) Kopf, S.; Bourriquen, F.; Li, W.; Neumann, H.; Junge, K.; Beller, M. Recent Developments for the Deuterium and Tritium Labeling of Organic Molecules. *Chem. Rev.* **2022**, *122*, 6634−6718. (g) Muthukrishnan, I.; Sridharan, V.; Menéndez, J. C. Progress in the Chemistry of Tetrahydroquinolines. *Chem. Rev.* **2019**, *119*, 5057−5191.
(26) Armarego, W. L. F.; Chai, C. Purification of Inorganic and Metal-Organic Chemicals. In *Purification of Laboratory Chemicals*, 7th ed.; Armarego, W. L. F., Chai, C., Eds.; Butterworth-Heinemann: Boston, 2013; Chapter 5, pp 555−661.
(27) (a) Yasmin, E.; Arora, V.; Kumar, A. An outlook on the applications of pincer-metal complexes in catalytic dehydrogenation chemistry. In *Pincer-Metal Complexes*; Kumar, A., Ed.; Elsevier, 2022; Chapter 5, pp 191−220. (b) Nandi, P. G.; Arora, V.; Yasmin, E.; Kumar, A. Pincer-group(8) and pincer-group(9) metal complexes for catalytic alkane dehydrogenation reactions. In *Pincer-Metal Complexes*; Kumar, A., Ed.; Elsevier, 2022; Chapter 2, pp 69−122. (c) Nandi, P. G.; Jadi, P. K.; Das, K.; Prathapa, S. J.; Mandal, B. B.; Kumar, A. Synthesis of NNN Chiral Ruthenium Complexes and Their Cytotoxicity Studies. *Inorg. Chem.* **2021**, *60*, 7422−7432.
(28) (a) Sheldrick, G. M. Crystal structure refinement with SHELXL. *Acta Crystallogr., Sect. A: Struct. Chem.* **2015**, *71*, 3−8. (b) Sheldrick, G. M. Crystal structure refinement with SHELXL. *Acta Crystallogr., Sect. C: Struct. Chem.* **2015**, *71*, 3−8.
(29) Perdew, J. P.; Burke, K.; Ernzerhof, M. Generalized Gradient Approximation Made Simple. *Phys. Rev. Lett.* **1996**, *77*, 3865−3868.
(30) Frisch, M. J.; Trucks, G. W., Schlegel, H. B.; Scuseria, G. E.; Robb, M. A.; Cheeseman, J. R.; Scalmani, G.; Barone, V.; Mennucci, B.; Petersson, G. A.; Nakatsuji, H.; Caricato, M.; Li, X.; Hratchian, H. P.; Izmaylov, A. F.; Bloino, J.; Zheng, G.; Sonnenberg, J. L.; Hada, M.; Ehara, M.; Toyota, K.; Fukuda, R.; Hasegawa, J.; Ishida, M.; Nakajima, T.; Honda, Y.; Kitao, O.; Nakai, H.; Vreven, T.; Montgomery, J. A., Jr.; Peralta, J. E.; Ogliaro, F.; Bearpark, M.; Heyd, J. J.; Brothers, E.; Kudin, K. N.; Staroverov, V. N.; Keith, T.; Kobayashi, R.; Normand, J.; Raghavachari, K.; Rendell, A.; Burant, J. C.; Iyengar, S. S.; Tomasi, J.; Cossi, M.; Rega, N.; Millam, J. M.; Klene, M.; Knox, J. E.; Cross, J. B.; Bakken, V.; Adamo, C.; Jaramillo, J.; Gomperts, R.; Stratmann, R. E.; Yazyev, O.; Austin, A. J.; Cammi, R.; Pomelli, C.; Ochterski, J. W.; Martin, R. L.; Morokuma, K.; Zakrzewski, V. G.; Voth, G. A.; Salvador, P.; Dannenberg, J. J.; Dapprich, S.; Daniels, A. D.; Farkas, O.; Foresman, J. B.; Ortiz, J. V.; Cioslowski, J.; Fox, D. J. *Gaussian 09*, Revision D.01; Gaussian, Inc.: Wallingford, CT, 2013.
(31) Hay, P. J.; Wadt, W. R. Ab Initio Effective Core Potentials for Molecular Calculations. Potentialsfor the Transition Metal Atoms Sc to Hg. *J. Chem. Phys.* **1985**, *82*, 270−283.

https://doi.org/10.1021/acscatal.2c05587
ACS Catal. 2023, 13, 3605−3617